



# Synthesis of Magnetic Biochar Using Agricultural Waste for the Separation of Cr(VI) From Aqueous Solution

Byomkesh Mahanty<sup>1</sup> · Sandip Mondal<sup>1</sup>

Received: 17 October 2020 / Accepted: 18 March 2021 / Published online: 5 April 2021  
© King Fahd University of Petroleum & Minerals 2021

## Abstract

The agricultural waste, i.e., peanut husk, was modified with iron oxide employed in Cr(VI) removal from wastewater. In this study, standard biochar ( $BC_{PH}$ ) was prepared from the pyrolysis process from peanut husk. The prepared biochar was magnetized by impregnating the iron oxide onto the surface of the biochar to enhance the adsorption capacity of the adsorbent. The morphological analysis and physicochemical properties of the synthesized biochar ( $BC_{PH}$ ) and magnetic biochar ( $MBC_{PH}$ ) were evaluated systematically by SEM, XRD, BET surface area ( $S_{BET}$ ) and point of zero charge ( $pH_{ZPC}$ ). Batch experiments were performed to evaluate the sorption mechanism and adsorption characteristics. The pH study revealed that maximum removal efficiency obtained in acidic condition ( $pH_{solution} < pH_{ZPC}$ ) of the solution. The pseudo-second-order reaction model is employed to kinetic data to determine the equilibrium time, maximum removal efficacy, and the adsorption rate constants of  $BC_{PH}$  and  $MBC_{PH}$ . The equilibrium time obtained at 90 min for  $MBC_{PH}$  and 150 min for  $BC_{PH}$ , and the corresponding maximum removal efficiency values are 95.27% and 45.56%, respectively. The isotherm data corroborated that the Freundlich model is the best fit model for both adsorbents. The maximum adsorption capacities were found 8.51 mg/g for  $BC_{PH}$  and 75.66 mg/g for  $MBC_{PH}$ , respectively. The results show that the uptake capacity of the  $MBC_{PH}$  is increased nine times compared to biochar ( $BC_{PH}$ ). The study concluded that the magnetic biochar ( $MBC_{PH}$ ) has higher uptake capacity and that can be used as a promising adsorbent for the separation of Cr(VI) from aqueous solution.

**Keywords** Magnetic biochar · Adsorption · Peanut husk · Regeneration · Chromium adsorption · Wastewater treatment

## 1 Introduction

Rapid growth in industrial sector has led to the degradation of water quality due to the discharge of inorganic pollutants such as heavy metals into the water bodies. Heavy metals pose high health risks due to high toxicity, carcinogenicity, and mobility in the water bodies [1]. Among few of the heavy metals which are toxic to the environment and human health, chromium is one of the major contaminants of industrial wastewater and mainly discharged to the environment from electroplating, nuclear power plant, textile industries, and leather tanning industries. Chromium exists in different oxidation states from +2 to +6 in the aqueous media. Among

them, Cr(VI) has high health risk that leads to organ damage, eye irritation, respiratory irritation, respiratory cancer, and discoloration of teeth to human beings, and animals through food intake and respiration [2, 3]. The Cr(VI) anions (i.e.,  $CrO_4^{2-}$ ,  $HCrO_4^-$ , and  $Cr_2O_7^{2-}$ ) are highly soluble, mobile, and toxic [1] thereby, the removal of it is a major challenge. Numerous treatment technologies have been developed for example chemical precipitation, ion exchange, membrane technologies, electrochemical treatment, and adsorption. However, adsorption has become the most cost-effective and worldwide accepted technique as many research works have been dedicated to develop low-cost and eco-friendly adsorbent to achieve a sustainable solution. Biosorbents are eco-friendly, abundantly available, easily synthesizable, and reduce the risk of generation of secondary pollutants [4]. Biochar is a porous, fine-grained, and carbonaceous material, and generally produced by pyrolysis of biomass at high temperature (250–1200 °C) in the absence of oxygen [4, 5].

The literature survey revealed that the biochar synthesized by agricultural waste has an affinity for Cr(VI) due to

✉ Sandip Mondal  
san.mondal@gmail.com

Byomkesh Mahanty  
b.mahanty95@gmail.com

<sup>1</sup> Department of Earth and Environmental Studies, National Institute of Technology Durgapur, Durgapur, India



its highly-porous structure, high specific surface area, and the presence of diverse functional groups (e.g., carboxyl, hydroxyl, and phenolic groups) [4]. Previous research studies the following adsorption capacity of biochar synthesized with agricultural waste for example, biochar derived from sugar beet tailings was 123 mg/g [6], for sewage sludge biochar was 64.1 mg/g [7], biochar derived from rice-husk was 23.1 mg/g [8], maximum adsorption capacity was found to be only 16.26 mg/g for peanut husk biochar [2, 3], 33.7 mg/g for Iron (III) and iminodiacetic acid functionalized magnetic peanut husk (Aaron et al. 2020). The sorption capacity of magnetic hollow sphere nanocomposite (graphene oxide-gadolinium oxide) has higher adsorption capacity 216.70 mg/g (Lakshmi et al. 2020). Corn husk derived magnetized activated carbon at 500 °C the adsorption was found about 96% and at 250 °C adsorption was 84% (Shubham et al. 2019). Separation of biochar from the aqueous solution is a critical issue for commercial applications due to the small particle sizes and lower density [9]. The problem can be overcome by modification of the biochar. Notably, the magnetization process can change the surface and porous structures of biochar and create additional adsorption sites, improving the adsorption capacity and separation potential [7, 9, 10]. Therefore, in this study, preparation of magnetic biochar with iron oxides using wasted peanut husk was synthesized to increase the adsorption capacity of hexavalent chromium.

## 2 Materials and Methods

### 2.1 Chemicals and Materials

Peanut husk was used as a biomass feedstock to synthesize of magnetic biochar, collected from the local market (Durgapur, India). The collected peanut husk was washed thoroughly using tap water followed by deionized (DI) water several times to remove the impurities and then placed in the hot air oven (Made by LABARD) for 24 h at a temperature of 80 °C to remove the moisture from the peanut husk and then crushed using a mixer grinder (Bajaj Rex 500-W mixer grinder). The crushed portion has been sieved through a 0.6-mm sieve shaker. Less than 0.6 mm size of particles were used to prepare magnetic biochar (MBC<sub>PH</sub>) by infusing FeCl<sub>3</sub>·6H<sub>2</sub>O by accomplishing the thermal process. Potassium dichromate (K<sub>2</sub>Cr<sub>2</sub>O<sub>7</sub>), sodium hydroxide (NaOH), Sodium Chloride (NaCl) and hydrochloric acid (HCL) were used as ingredients during the batch experimental studies. All the chemicals were analytical grade and used without any further purification. Deionized (DI) water was used for the preparation of all the reagents and standards. Synthetic 1000 mg/L of hexavalent chromium [Cr(VI)] stock solution was prepared using Potassium dichromate

(K<sub>2</sub>Cr<sub>2</sub>O<sub>7</sub>) salt. Cr(VI) standard solutions were prepared from the stock solution by serial dilution method to conduct the batch experiments.

### 2.2 Synthesis of magnetic biochar

Magnetic biochar was synthesized employing the modified method proposed by Liu et al. [9]. The synthesis procedure for magnetic biochar is depicted in Fig. 1. Initially, 10 gm of dried peanut husk was immersed into 80 ml of FeCl<sub>3</sub>·6H<sub>2</sub>O solution at a mixing ratio of 1:8(w/v). After vigorously mixing for 1 hour using a magnetic stirrer, Fe<sup>3+</sup> precipitation was accelerated by aging at a temperature of 60 °C for 0.5 h. After that, the pre-treated biomass, i.e., peanut husk, was filtered using Whatman 42 filter paper, and the residue was kept in the hot air oven for 24 h at a temperature of 70 °C. The dried pre-treated biomass was then pyrolysis in a tube furnace under N<sub>2</sub> atmosphere for 2 h at 600 °C. The peak temperature was reached using a heating rate of 15 °C/min. After cooling down, the magnetic biochar was washed several times using deionized (DI) water and ethanol simultaneously to remove the ashes and impurities. The magnetic biochar was then placed in a vacuum oven (MTI corporation, California, USA) at 70 °C for 24 h to make it completely dry. This prepared magnetic biochar is stored in a sealed container for further use. Standard biochar (BC<sub>PH</sub>) was prepared in the same way without treated by FeCl<sub>3</sub>·6H<sub>2</sub>O solution.

### 2.3 Characterization

#### 2.3.1 Proximate Analysis

The proximate analysis was carried out by modified thermal analysis methods to determine the moisture, ash, volatile matter, and fixed carbon content of the Biochar (BC) samples [11]. A fixed amount of samples was taken in crucibles and placed in a Hot air oven at 105 °C for 1.5 h. The weight loss of the samples was measured, and the moisture content of the samples was determined. The oven-dried samples were kept in a muffle furnace in a crucible at 750 °C for 1.5 h to evaluate the ash content. The percentage loss of weight represents the ash content. To determine the volatile matter content (non-carbonized portion), the oven-dried BC samples were kept in the muffle furnace in a crucible with lid cover at 920 °C for precisely 7 min and measured percentage of the weight difference between initial to final weight with respect of oven-dry weight.

#### 2.3.2 Surface Area and Morphological Analysis

Brunauer, Emmett, and Teller's theory is applied to determine the surface area of porous powdered solid particles [12]. The specific surface areas of BC samples were

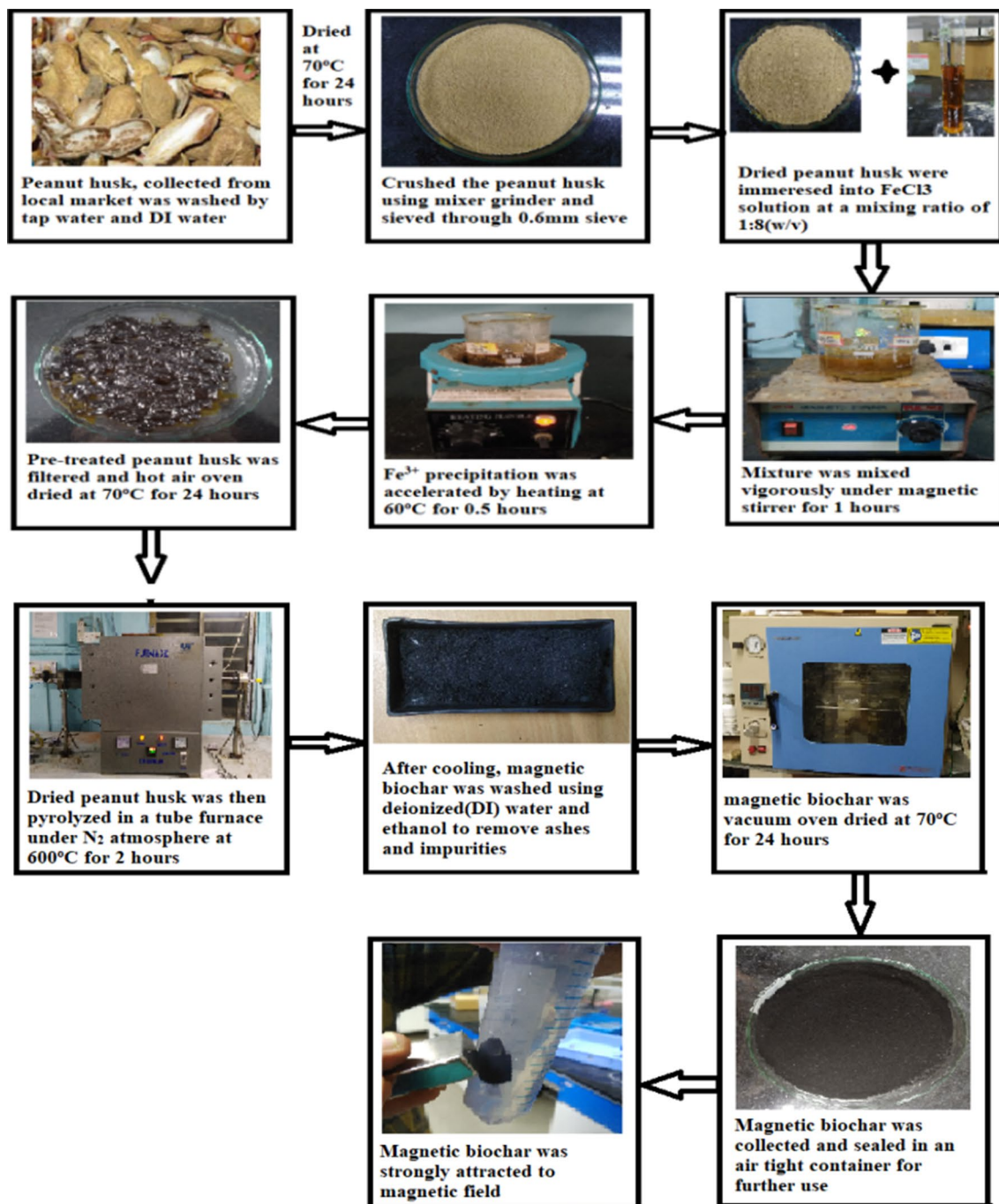


**Fig. 1** Synthesis procedure of magnetic biochar (MBC<sub>PH</sub>)

measured by N<sub>2</sub> adsorption–desorption isotherms at 77 K by Brunauer–Emmett–Teller surface area analyser (NOVA 1200e, Quanta chrome). The BC samples were degassed at 300 °C under vacuum for 3 h to conduct gas adsorption measurement. At a relative pressure, around 0.95, the pore volume was obtained from the amount of nitrogen adsorbed [12]. FE-SEM (Field Emission Scanning Electron Microscope) (S-3000 N, Hitachi, Japan) was used at

an electron acceleration voltage of 30 kV (Carl Zeiss AG) to determine the surface structure and morphology of the BC samples. A small amount of BC samples was fixed on a sample holder by the conductive carbon glue and, after that, allowed to dry on the heating plate. The BC samples’ surfaces were coated with a thin layer of gold sputter coater to make them conductive.

### 2.3.3 Elemental and Crystallographic Analysis

Elemental analysis of the BC samples was carried out to estimate Carbon/hydrogen/oxygen/nitrogen/sulfur contents into the BC samples and the raw feedstock. The crystallographic structure of the BC samples was examined by X-ray diffraction (XRD) with Cu and K $\alpha$  radiation, and the samples were scanned in the range of 10–90° (2 $\theta$ ) with a scan speed of 2 °C/min.

### 2.3.4 Point of Zero Charge (pH<sub>ZPC</sub>) Test

The pH<sub>ZPC</sub> test was conducted for MBC<sub>PH</sub> and BC<sub>PH</sub> using 0.01 M NaCl solutions at 2–12 pH. The pH values of the solutions were adjusted by using 0.1 M HCl and 0.1 M NaOH solution. 0.02 g of adsorbent was added to 50 ml of each solution and was kept in BOD incubator shaker at 150 rpm agitation speed at 25 °C temperature for 24 h. Then pH of the supernatant was measured. The plot of initial solution pH vs. pH of the supernatant gives the value of pH<sub>ZPC</sub>.

## 2.4 Adsorption Studies

To determine the removal efficiency, uptake capacity, and process mechanism, the batch experimental studies have been carried out for both adsorbents, i.e., magnetic biochar (MBC<sub>PH</sub>) and standard biochar (BC<sub>PH</sub>). To conduct the isotherm studies, varying adsorbent doses (0.025–0.4 g/50 ml) were added to separate beakers containing 50 ml of 50 mg/L Cr(VI) solution. The samples were placed in the BOD incubator shaker at 150 rpm agitation speed at 25 °C temperature. The initial pH values of the samples were adjusted to 2.0 using 0.1 M HCl and 0.1 M NaOH solution. The kinetic study was conducted by varying the contact time (1–180 min) with the adsorbent dose of 0.2 g/50 ml. The other parameters are maintained constant as similar to the isotherm study. Similarly, the effects of initial adsorbate concentration study was carried out by the varying initial concentration (30–90 mg/L) of Cr(VI) in the solution. The effect of solution pH on Cr(VI) removal was investigated under initial pH of 2–10. After conducting the batch experiments, the samples were separated using a vacuum filter and preserved at less than pH 2 for further analysis. The Cr(VI) concentration of the samples were measured using AAS (Atomic absorption spectroscopy) in flame mode. The amount of Cr(VI) adsorbed per unit adsorbent ( $q_e$ , mg/g) and the removal efficiency ( $R$ , %) was calculated according to the following equations [13] [2, 3].

$$q_e = \frac{(C_0 - C_e)V}{m} \quad (1)$$

$$R = \frac{(C_0 - C_e)}{C_0} \times 100\% \quad (2)$$

In the regeneration experiment, 0.2 g adsorbent was added into 50 mL Cr(VI) solution (50 mg/L, pH=2.0) in a beaker at an agitation rate of 150 rpm at room temperature (25 °C) for 3 h. After the adsorption, the Cr(VI) loaded adsorbent was filtered by Whatman 42 filter paper and washed several times with deionized (DI) water and then kept in contact with 50 ml of 0.1 M NaOH solution and then again washed with deionized (DI) water [14] and dried in vacuum oven for the next adsorption experiment.

## 2.5 Effects of Coexisting Ions

The effects of coexisting ions have been investigated at equilibrium condition at 25 °C. Different electrolytes such as NaNO<sub>3</sub>, Mg(NO<sub>3</sub>)<sub>2</sub>·6H<sub>2</sub>O, Al(NO<sub>3</sub>)<sub>3</sub>·9H<sub>2</sub>O, NaCl, NaHCO<sub>3</sub>, Na<sub>2</sub>SO<sub>4</sub> and Na<sub>2</sub>HPO<sub>4</sub>·2H<sub>2</sub>O were added at different strength (0.01, 0.05, 0.1, 0.15 M) separately to a solution containing 50 ml, 50 mg/L of Cr(VI). After completion of the experiments, the concentration of the effluent samples were estimated to observed the effects of the coexisting ions.

## 2.6 Adsorption Isotherm Models

To describe the adsorption system of the adsorbents and adsorption mechanism adsorption isotherm study is important. Relation between the remaining concentration of solute in the liquid phase and the amount of solute adsorbed by the unit mass of adsorbent are expressed in adsorption isotherms. Therefore, it is necessary to establish the equilibrium relation between the solid phase and liquid phase concentration of Cr(VI) at equilibrium condition. In this study, the adsorption capacity of Cr(VI) by BC samples was investigated with the Langmuir [15], Freundlich [16], Temkin [17] and Dubinin–Radushkevich (D–R) [18] adsorption isotherms.

### 2.6.1 Langmuir Isotherm

Previously for the adsorption of heavy metals, dyes, organic pollutants, Langmuir isotherm has been widely used [19, 20]. Langmuir isotherm is one-molecular layer adsorption. In this isotherm all sites have equal adsorbate affinity and the adsorbed molecule does not affect the adsorption at neighboring site [15, 21]. The maximum adsorption capacity obtains from the Langmuir isotherm. The isotherm equation can be represented as given by Eq. (3):

$$\frac{q_e}{q_m} = \frac{bC_e}{1 + bC_e} \quad (3)$$

where  $C_0$  is the initial concentration of the adsorbate (mg/L),  $b$  is adsorption equilibrium constant that is related to the Henry constant ( $K_L = bq_m$ ),  $q_m$  is the maximum adsorption capacity of the adsorbent (mg/g),  $q_e$  is the amount adsorbed

on unit mass of the adsorbent (mg/g), when the equilibrium concentration is  $C_e$  (mg/L). Equation (3) can be rearranged as given by Eq. (4) [22]:

$$\frac{C_e}{q_e} = \frac{1}{bq_m} + \frac{C_e}{q_m} \quad (4)$$

The value of Langmuir constant can be estimated from the plot of  $C_e/q_e$  versus  $C_e$ .

### 2.6.2 Freundlich isotherm

This isotherm model says that in different concentrations, the ratio of adsorbate adsorbed onto a given mass of adsorbent to the concentration of adsorbate in the solution is not constant [21]. This model proposes multilayer adsorption with a heterogeneous energetic distribution of active sites, accompanied by interaction between adsorbed molecules [16, 23]. The isotherm equation can be represented as given by Eq. (5):

$$q_e = K_f C_e^{1/n} \quad (5)$$

where,  $K_f$  ( $\text{mg}^{1-1/n} \text{L}^{1/n} \text{g}^{-1}$ ) is the adsorption capacity of the adsorbent,  $n$  is the constant depending on the heterogeneity properties of the adsorbent. The equation can be expressed in linear form as given by Eq. (6) [16, 24]:

$$\ln q_e = \ln K_f + \left(\frac{1}{n}\right) \ln C_e \quad (6)$$

The value of  $n$  and  $K_f$  can be estimated from the plot of  $\ln q_e$  versus  $\ln C_e$ .

### 2.6.3 Temkin Isotherm

This isotherm is based on a factor that takes into account of the adsorbent–adsorbate interactions. The assumption is that the heat of adsorption of all the molecules in the layer decreases linearly with the coverage of molecules due to the adsorbate–adsorbate interaction [21].

Another one assumption is that the fall in the heat of adsorption is linear rather than logarithmic [17, 25]. The Temkin isotherm equation can be represented as given by Eq. (7) [21]:

$$\frac{q_e}{q_m} = B \ln A + B \ln C_e \quad (7)$$

where  $B = RT/\Delta Q$ ,  $R$  is universal gas constant ( $8.314 \text{ J mol}^{-1} \text{ K}^{-1}$ ),  $T$  is the absolute temperature ( $K$ ),  $\Delta Q$  is the energy transmission during adsorption ( $\text{KJ mol}^{-1}$ ) and  $A$  ( $K_0$ ) is the Temkin constant ( $\text{L/mg}$ ).

The value of  $A$  and  $B$  can be estimated from the plot of  $q_e/q_m$  versus  $\ln C_e$ .

### 2.6.4 Dubinin–Radushkevich (D–R) Isotherm

Dubinin and Radushkevich have proposed another isotherm model. It is not about homogeneous surface or constant adsorption potential. This isotherm model is applicable for estimating the mean free energy of sorption ( $E_D$ ). Physical adsorption prevails, if the value of  $E$  less than  $16 \text{ kJ mol}^{-1}$ , and chemisorption prevails, if the value of  $E$  is more than  $16 \text{ kJ mol}^{-1}$  [18, 21]. The non-linear form of this isotherm can be represented by the Eq. (8):

$$\log_{10}^{q_e} = \log_{10}^{q_D} - 2B_D R^2 T^2 \log_{10} \left( 1 + \frac{1}{C_e} \right) \quad (8)$$

where  $q_D$  is theoretical saturation capacity ( $\text{mg g}^{-1}$ ) and  $B_D$  is a constant related to adsorption energy ( $\text{mol}^2 \text{ kJ}^{-2}$ ),  $R$  is universal gas constant ( $8.314 \text{ J mol}^{-1} \text{ K}^{-1}$ ),  $T$  is the absolute temperature ( $K$ ).

The value of the mean free energy of sorption ( $E_D$ ) can be calculated from Eq. (9):

$$E_D = 1/(2B_D)^{0.5} \quad (9)$$

The value of  $q_D$  and  $B_D$  can be estimated from the plot of  $\log_{10} q_e$  versus  $\log_{10}(1 + 1/C_e)$ .

## 2.7 Adsorption Kinetics

Kinetic models have employed to explain the removal process of Cr(VI) and to determine the rate of sorption mechanism from the aqueous solution. The kinetics of Cr(VI) removal were analysed by pseudo-first-order, pseudo-second-order, Elovich and Weber and Morris models [26–28].

### 2.7.1 Pseudo-First-order Kinetics

Pseudo-first-order reaction model showed that the adsorbate adsorption rate on the adsorbent is based on the adsorption capacity [27]. The linear form of pseudo-first-order kinetic equation can be represented as given by Eq. (10):

$$\ln \left[ \frac{(q_e - q_t)}{q_e} \right] = -k_1 t \quad (10)$$

where  $k_1$  ( $\text{min}^{-1}$ ) is the adsorption operation rate constant of the pseudo-first-order model,  $q_e$  is the adsorbed amounts of adsorbate ( $\text{mg g}^{-1}$ ) at equilibrium time and  $q_t$  is the adsorbed amounts of adsorbate ( $\text{mg g}^{-1}$ ) at any instant of time,  $t$ . The value of  $k_1$  can be obtained from the plot of  $\ln[(q_e - q_t)/q_e]$  versus  $t$ .



### 2.7.2 Pseudo-Second-order Kinetics

As only the value of  $k_1$  can be obtained from pseudo-first-order kinetic model, and it cannot obtain the value of  $q_e$ . Therefore, for the estimation of the value of  $q_e$  pseudo-second-order kinetics has to be tested. Pseudo-second-order kinetic equation can be represented as given by Eq. (11) [27]:

$$\frac{t}{q_t} = \frac{1}{k_2 q_e^2} + \frac{t}{q_e} \quad (11)$$

where  $k_2$  ( $\text{gm g}^{-1} \text{min}^{-1}$ ) is the rate constant of pseudo-second-order kinetic model. The value of  $k_2$  and  $q_e$  can be obtained from the linear plot of  $t/q_t$  versus  $t$ .

### 2.7.3 Elovich Kinetic Model

Elovich kinetic model basically express the adsorption capacity rate. This equation can be represented as given by Eq. (12) [26]:

$$q_t = \beta \ln(\alpha\beta) + \beta \ln t \quad (12)$$

where  $\alpha$  ( $\text{mg g}^{-1} \text{min}^{-1}$ ) is initial sorption rate of Cr(VI) species,  $\beta$  ( $\text{gm g}^{-1}$ ) is the desorption constant during one experiment.

The value of the kinetic constant  $\alpha$  and  $\beta$  can be estimated from the plot of  $q_t$  versus  $\ln t$ .

### 2.7.4 Weber and Morris Kinetic Model

Weber and Morris developed the intra particle diffusion model or parabolic diffusion model which also used to describe the adsorption kinetics. Pseudo-second-order kinetic equation can be represented as given by Eq. (13) [27, 29]:

$$q_t = k_d \times t^{0.5} + c \quad (13)$$

where  $k_d$  is the intra particle diffusion rate constant ( $\text{mg g}^{-1} \text{min}^{-1/2}$ ),  $c$  ( $\text{mg g}^{-1}$ ) is the constant which gives an idea about the boundary layer thickness.

The value of  $k_d$  and  $c$  can be estimated from the plot of  $q_t$  versus  $t^{0.5}$ .

## 3 Result and Discussion

### 3.1 Characterization

The results of proximate analysis of Raw peanut husk (feedstock peanut husk of particle size  $< 0.6$  mm),  $\text{BC}_{\text{PH}}$ ,  $\text{MBC}_{\text{PH}}$  are shown in Table 1. From the result, it is clear that the fixed carbon content and ash content have been increased

after pyrolysis of the biochar. This may be due to the mineral's condensation and volatilization of organic matters; as a result, ash content was increased. Again, in case of  $\text{MBC}_{\text{PH}}$ , iron was impregnate to the surface of the  $\text{BC}_{\text{PH}}$  which enhances the inorganic carbon content. Fixed carbon content of  $\text{MBC}_{\text{PH}}$  was slightly decreased may be due to the increase in iron (Fe) content which led to decrease in carbon content. The volatile matter was declined for may be due to loss of organic matter at very high temperature as well as the amorphous phase loss.

The result of elemental analysis raw peanut husk,  $\text{BC}_{\text{PH}}$ ,  $\text{MBC}_{\text{PH}}$  are given in Table 2. From the result, it is clear that the carbon content on the biochar samples was higher than raw peanut husk due to high carbonization. But carbon content on the  $\text{MBC}_{\text{PH}}$  was slightly lower than  $\text{BC}_{\text{PH}}$  may be due to the presence of iron content. The hydrogen and oxygen contents were declined after pyrolysis, which can be explained by cracking of bonds and degradation of raw material. Similarly, nitrogen content decreased for both the biochar sample. However, sulfur content for both the biochar sample was negligible ( $< 0.1\%$ ).

One of the most important physical factors of biochar is BET surface area which affects heavy metals adsorption. The result of BET analysis of raw peanut husk,  $\text{BC}_{\text{PH}}$ , and  $\text{MBC}_{\text{PH}}$  are summarized in Table 2. It can be seen that the BET surface area of  $\text{MBC}_{\text{PH}}$  is higher compared to the  $\text{BC}_{\text{PH}}$ . Surface area of biochar is increased from 16.48 to 183.62  $\text{m}^2/\text{g}$  after magnetization with iron oxides. This may be due to the doped iron oxides particles on to the surface of biochar. As iron oxide particles are itself nanomaterial, which attributed to enhance the surface area. Because in general smaller the particle size, larger the surface area. Similar type of trends was noted in previous studies [5, 30]. On the other hand, it can be noticed that the pore volume was also increased from 0.132 to 0.263  $\text{cm}^3/\text{g}$  after magnetization of the biochar. Increased of surface area and pore volume cater more adsorption sites which enhances the removal efficiency of Cr(VI).

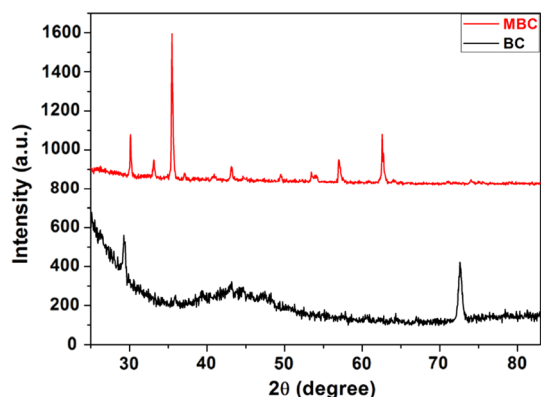
The XRD analysis was carried out to investigate the phase structure and crystallographic characteristic of  $\text{BC}_{\text{PH}}$  and  $\text{MBC}_{\text{PH}}$ . The intensity pattern of the biochar samples is shown in Fig. 2. It can be observed that various peaks at  $14.8^\circ$ ,  $16.7^\circ$  and  $29.3^\circ$  appear for the pattern of  $\text{BC}_{\text{PH}}$  with corresponding crystal index planes 110, 002, and 103, respectively. Matching with the XRD standard card (JCPDS

**Table 1** Proximate analysis (wt%) of raw peanut husk,  $\text{BC}_{\text{PH}}$ ,  $\text{MBC}_{\text{PH}}$

Samples	Moisture	Ash	Volatile matter	Fixed carbon
Raw PH	8.13	3.91	76.48	11.48
$\text{BC}_{\text{PH}}$	1.91	15.23	6.79	76.07
$\text{MBC}_{\text{PH}}$	2.53	20.19	4.27	73.01

**Table 2** Elemental composition (wt%), BET surface area, and pore volume of raw peanut husk, BC<sub>PH</sub>, MBC<sub>PH</sub>

Samples	C	H	O	S	N	Surface area (m <sup>2</sup> /g)	Pore volume (cm <sup>3</sup> /g)
Raw PH	45.21	5.39	42.39	0.61	0.44	1.81	0.011
BC <sub>PH</sub>	84.34	1.93	2.16	0.08	0.26	16.48	0.132
MBC <sub>PH</sub>	82.61	1.39	1.74	0.06	0.21	183.62	0.263

**Fig. 2** XRD spectra of BC<sub>PH</sub> and MBC<sub>PH</sub>

Card No. 50–0926), the pattern of BC<sub>PH</sub> indicated that BC<sub>PH</sub> is made of amorphous carbon. Moreover, it is also observed that various sharp peaks at 30.2°, 35.5°, 43.2°, 57.3° and 62.9° appear for the pattern of MBC<sub>PH</sub> with corresponding crystal index planes 220, 311, 400, 511 and 440 respectively. Matching with the XRD standard card (JCPDS Card No. 39–1346) confirms that  $\gamma$ -Fe<sub>2</sub>O<sub>3</sub> was successfully formed on the surface of MBC<sub>PH</sub>. However, the peaks at 32.2° with corresponding crystal index plane 104 attributed to  $\alpha$ -Fe<sub>2</sub>O<sub>3</sub> [2, 3, 30]. Huge number of  $\gamma$ -Fe<sub>2</sub>O<sub>3</sub> particles covered the surface of the MBC<sub>PH</sub> that is why there was no peak of amorphous carbon.

SEM analysis was conducted to investigate the morphological structure of the MBC<sub>PH</sub> and BC<sub>PH</sub> as shown in Fig. 3. The figure shows (Fig. 3a) that the BC<sub>PH</sub> surface contains abundant pores with diverse shape and size, as well as the surface of the BC<sub>PH</sub> is rough. In contrast, morphological analysis (Fig. 3b) also revealed that irregular iron oxide particles dispersed on the surface of the MBC<sub>PH</sub>. It was observed that the pores of the MBC<sub>PH</sub> were blocked due to the formation of iron oxide which helped to keep the rugged surface structure of MBC<sub>PH</sub>. Figure 3c shows that Cr(VI) was successfully adsorbed on to the surface of magnetic biochar (MBC<sub>PH</sub>).

The literature revealed the FTIR pattern of MBC<sub>PH</sub> and BC<sub>PH</sub>. It was observed that there exist some peaks, such as carboxyl and hydroxyl group (attributed to –OH) vibration at around 3384 cm<sup>-1</sup>, C=O vibration at around 2858 cm<sup>-1</sup>,

aromatic (attributed to C=C) vibration at around 1628 cm<sup>-1</sup>, N–C=O vibration at 1452 cm<sup>-1</sup>, –COOH group vibration at around 1368 cm<sup>-1</sup>, alcoholic group (attributed to CO–) vibration at around 1058 cm<sup>-1</sup>, phenolic group vibration at around 1267 cm<sup>-1</sup>. The peak at around 582 cm<sup>-1</sup> presents Fe–O bond vibration [2, 3, 30]. It may be possible that the magnetic biochar surfaces covered with iron oxide particles. Similar functional groups will exist in MBC<sub>PH</sub> and BC<sub>PH</sub> which was used in this study. Therefore, abundant active functional groups are present on the surface of biochar samples and thus they have high adsorption capacity.

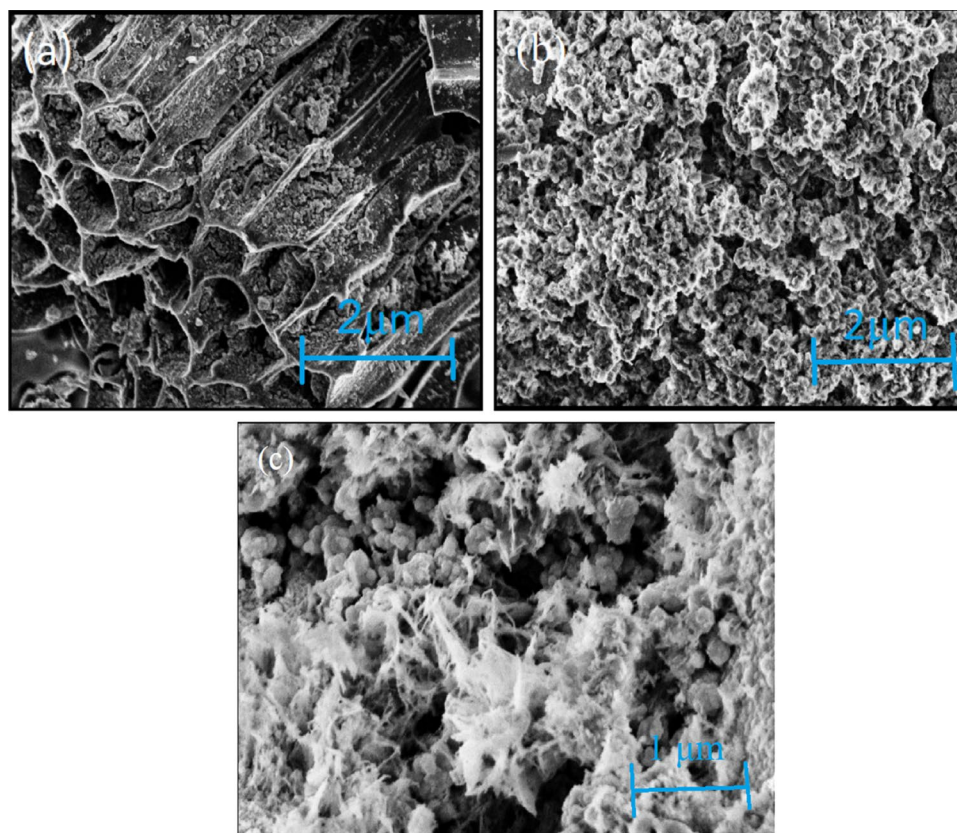
The point of zero charge (pH<sub>ZPC</sub>) is an important aspect to understand adsorbent behavior in the solution. From the findings it can be seen that the pH<sub>ZPC</sub> values were obtained 2.65 and 6.5 for MBC<sub>PH</sub> and BC<sub>PH</sub> respectively. The result revealed that the MBC<sub>PH</sub> was acidic nature. This may be due to the existence of carboxyl and phenolic group and iron impregnation on the surface of the adsorbent.

## 3.2 Adsorption Study for Cr(VI) Removal

### 3.2.1 Effect of Adsorbent dose on Cr(VI) Adsorption

The heavy metal removal is a function of adsorbent dosage as it determines the adsorbent capacity to remove an adsorbate for a given initial concentration. Therefore, the removal efficiency of BC<sub>PH</sub> and MBC<sub>PH</sub> was determined at different adsorbent doses for the per cent removal of Cr(VI) ions. The effect of adsorbent dose on Cr(VI) removal is shown in Fig. 4a and it can be seen that the removal efficiency of Cr(VI) ions increased from 53.52 to 96.22% for MBC<sub>PH</sub> and 7.04% to 62.44% for BC<sub>PH</sub> with various adsorbent doses from 0.025 g to 0.4 g/50 ml. The removal of Cr(VI) increases with adsorbent dose is due to the increasing in surface area and the availability of more adsorption sites. But with further increase in adsorbent dose, there decreased in adsorption efficiency for both the adsorbents. 0.2 g/50 ml adsorbent dose was found to be optimum dose for the removal of Cr(VI) because with further increasing doses there slightly increased adsorption efficiency and then decreased. Therefore, rest of the study was conducted using 0.2 g/50 ml adsorbent dose. Furthermore; the q<sub>e</sub> value for Cr(VI) was reduced from 53.52 to 6.01 mg/g for MBC<sub>PH</sub> and from 7.04 to 3.90 mg/g for BC<sub>PH</sub> by increasing in the adsorbent dose

**Fig. 3** SEM image of **a**  $BC_{pH}$ ; **b**  $MBC_{pH}$  and **c** after adsorption of Cr(VI) by  $MBC_{pH}$



from 0.025 g to 0.4 g/50 ml. It can be explained as the overcrowding of adsorbent particles reduced the adsorption sites for Cr(VI) adsorption on the surface of the adsorbent.

### 3.2.2 Effect of Contact Time on Cr(VI) Adsorption

To determine the influence of the optimal contact time and adsorption kinetics, the sorption behavior of Cr(VI) on the adsorbents  $BC_{pH}$  and  $MBC_{pH}$  were studied at a fixed dose of adsorbent 0.2 g/50 ml for 1 to 180 min, while keeping other parameters constant. The effects of the contact time on Cr(VI) removal is shown in Fig. 4b. It can be seen that the removal efficiency of Cr(VI) ions reaches up to 95.27% for  $MBC_{pH}$  and 45.56% for  $BC_{pH}$  respectively within 180 min. It was observed that the adsorption equilibrium was established in 90 min for  $MBC_{pH}$  and 150 min for  $BC_{pH}$ . Then the adsorption rate remains constant up to 180 min of contact time for both the adsorbents. The maximum  $q_e$  value obtained for Cr(VI) removal was 11.91 mg/g for  $MBC_{pH}$  and 5.69 mg/g for  $BC_{pH}$ . Higher adsorption rate observed before reaching to the adsorption equilibrium for both the adsorbents, this may be due to the availability of a large number of active adsorption sites on the surface of the adsorbents for Cr(VI) ions sorption and fast ion-reduction with the help of oxygen-containing functional groups present on the surface of the adsorbents. After reaching the equilibrium, there was

no significant change on removal of Cr(VI) and that might be due to the saturation of adsorption sites available on the adsorbent surfaces.

### 3.2.3 Effect of Initial Concentration on Cr(VI) Adsorption

The effect initial adsorbate concentration ( $C_0$ ) has been investigated and the obtained results are depicted in Fig. 4c. It is clear that the removal of Cr(VI) decreased with increasing in initial chromium concentration for both the adsorbents. It was shown that the removal efficiency decreased from 96.95 to 76.20% for  $MBC_{pH}$  and from 58.72 to 6.20% for  $BC_{pH}$ . The reason behind this may be due to the incising in Cr(VI) concentration in the solution, decreasing in the binding capacity of the adsorbent which leads to decreased in Cr(VI) sorption. There is less number of active adsorption sites are available at higher concentration of adsorbate.

### 3.2.4 Effect of pH on Cr(VI) Adsorption

The pH value of the solution plays an important role for the removal of Cr(VI) ions as because of pH can influence the present form of chromium in the solution, as well as the property of adsorbents. The removal percentage of Cr(VI) ions was examined with different pH ranges from 2 to 10, while keeping other parameters constant. From Fig. 4d,



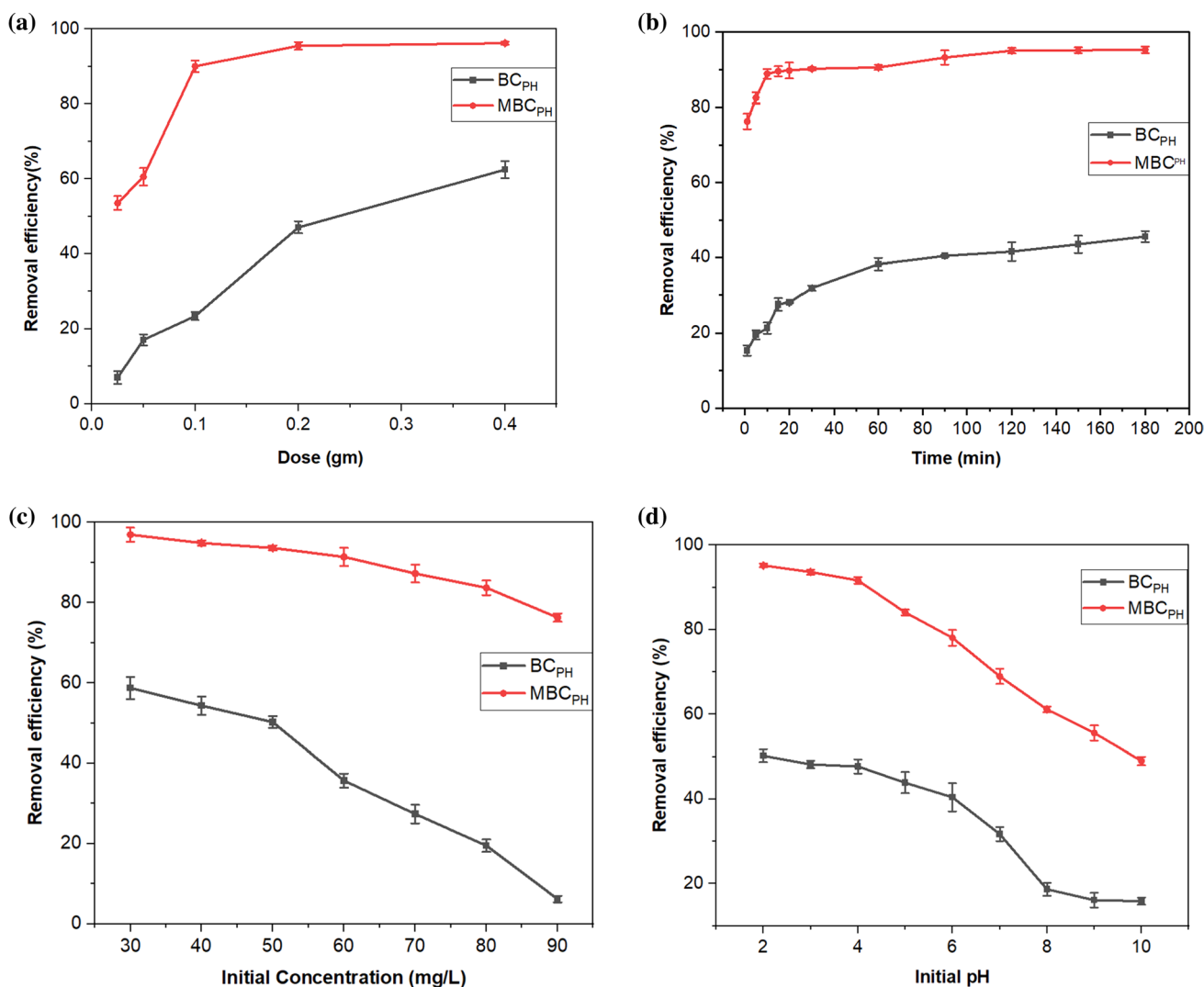
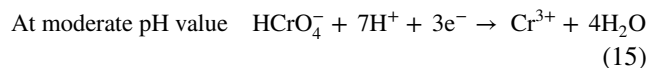
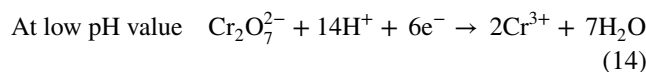


**Fig. 4** Effect of **a** adsorbent dose, **b** adsorption time, **c** initial concentration of Cr(VI) and **(d)** initial pH of solution on removal of Cr(VI) by MBC<sub>PH</sub> and BC<sub>PH</sub>

it can be seen that the removal of Cr(VI) decreased with increasing in solution pH, the removal of Cr (VI) found maximum at lower pH value for both the adsorbents (BC<sub>PH</sub> and MBC<sub>PH</sub>). High removal efficiency was obtained for Cr(VI) ions at pH 2, for both the adsorbents. As the solution pH move from acidic to basic, the removal efficiency decreased rapidly from 95.19% to 49.03% for MBC<sub>PH</sub> and from 50.04 to 15.88% for BC<sub>PH</sub>. Furthermore, the adsorption capacity for Cr(VI) was reduced from 11.899 to 6.127 mg/g for MBC<sub>PH</sub> and from 7.03 to 1.235 mg/g for BC<sub>PH</sub> respectively. It may be possible that as Cr(VI) present in aqueous solution in different ionic forms, such as HCrO<sub>4</sub><sup>-</sup>, Cr<sub>2</sub>O<sub>7</sub><sup>2-</sup>, and CrO<sub>4</sub><sup>2-</sup>, which directly depends on the redox condition of the solution and the concentration level of Cr (VI) ions. Normally, HCrO<sub>4</sub><sup>-</sup> is the predominant species at pH 2.0–5.0 range. While at high pH values, CrO<sub>4</sub><sup>2-</sup>, HCrO<sub>4</sub><sup>-</sup>,

Cr<sub>2</sub>O<sub>7</sub><sup>2-</sup> and Cr<sub>3</sub>O<sub>10</sub><sup>2-</sup> ions readily adsorbs on the surfaces of the adsorbents due to their low adsorption free energy [31]. At low pH condition, the removal capacity of the adsorbents for Cr(VI) was found higher may be due to the reduction of Cr(VI) to Cr(III):



Again, at lower pH, H<sup>+</sup> ions are the dominating species in the solution and that contribute to the removal of Cr(VI) by increasing the positive surface charge of the BC<sub>PH</sub> and MBC<sub>PH</sub>. Thus, at very low pH (pH<sub>solution</sub> < pH<sub>zpc</sub>) condition of the solution, anionic form of Cr(VI) can easily be

adsorbed onto the positively charged adsorbents surface through electrostatic attraction. However, with the increasing of pH of the solution leads to increasing of the  $\text{OH}^-$  concentration which introduced competitive adsorption with Cr(VI) species. As a result, at higher pH value of the solution,  $\text{BC}_{\text{PH}}$  and  $\text{MBC}_{\text{PH}}$  show lower removal efficiency.

### 3.2.5 Effect of Temperature on Cr(VI) Adsorption

The effect of the temperature for the Cr(VI) removal has been investigated for both adsorbents and the corresponding obtained results are depicted in Fig. 5. It can be seen that the sorption capacity of Cr(VI) increased with increasing temperature from 15 to 45 °C for both the adsorbents (i.e.,  $\text{BC}_{\text{PH}}$  and  $\text{MBC}_{\text{PH}}$ ), while keeping other parameters constant. The results corroborate that the maximum removal efficiency of Cr(VI) ions was found 97.97% at 45 °C for  $\text{MBC}_{\text{PH}}$  and 60.96% at 45 °C for  $\text{BC}_{\text{PH}}$  respectively. The reason behind this may be due to the required temperature is high to activate the available adsorption sites on the surface of the adsorbents. Furthermore, the maximum adsorption capacity for Cr(VI) was obtained 12.25 mg/g for  $\text{MBC}_{\text{PH}}$  and 7.62 mg/g for  $\text{BC}_{\text{PH}}$ . Consequently, from the assumption of Freundlich isotherm model, it can be concluded that heterogeneous energetic distribution of active sites are available for sorption of Cr(VI), accompanied by interaction between adsorbed molecules.

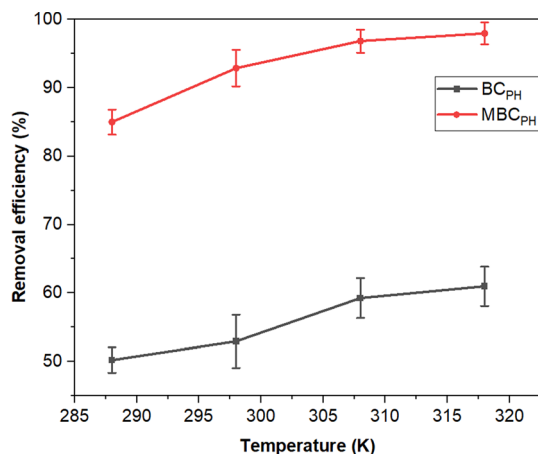


**Fig. 5** Effect of temperature on removal of Cr(VI) by  $\text{BC}_{\text{PH}}$  and  $\text{MBC}_{\text{PH}}$

**Table 3** Isotherm models constants and correlation coefficients data

Adsorbents	Langmuir isotherm			Freundlich isotherm			Temkin isotherm		
	$b$ (L/mg)	$K_L$ (L/g)	$R^2$	$K_f$ ((mg/g) (L/mg) <sup>1/n</sup> )	$n$	$R^2$	$A$ (L/mg)	$B$	$R^2$
$\text{BC}_{\text{PH}}$	0.0155	0.0863	0.5105	0.496	1.3765	0.8466	0.1456	0.5868	0.8061
$\text{MBC}_{\text{PH}}$	0.0734	0.2045	0.6522	5.796	1.533	0.8578	0.9248	0.2658	0.834

### 3.3 Adsorption Isotherms

In methodology section, theory of the isotherm models was described. It was observed from the results of the isotherm models (Table 3) of Cr(VI) adsorption by  $\text{BC}_{\text{PH}}$  and  $\text{MBC}_{\text{PH}}$  that Freundlich isotherm model (Fig. 6b) was best fitted model compared to Langmuir (Fig. 6a) and Temkin (Fig. 6c) isotherm model for the sorption of Cr(VI) according to the value of coefficient of correlation ( $R^2$ ) 0.8466 and 0.8578 for  $\text{BC}_{\text{PH}}$  and  $\text{MBC}_{\text{PH}}$ , respectively. The adsorption capacity obtained from the result was 8.507 mg/g and 75.656 mg/g for  $\text{BC}_{\text{PH}}$  and  $\text{MBC}_{\text{PH}}$ , respectively. Therefore,  $\text{MBC}_{\text{PH}}$  showed higher adsorption capacity compared to  $\text{BC}_{\text{PH}}$ .

The results obtained from Dubinin–Radushkevich (D–R) isotherm model (Fig. 7a,b) are given in Table 4. From the result, it can be seen that the  $E_D$  values were 5.492 kJmol<sup>-1</sup> for  $\text{MBC}_{\text{PH}}$  and 0.0813 kJmol<sup>-1</sup> for  $\text{BC}_{\text{PH}}$ .  $E_D$  value less than 16 kJ mol<sup>-1</sup> as indicated by our results shows that the sorption process of hexavalent chromium follows physical adsorption.

### 3.4 Adsorption Kinetics

Theory of the kinetic models was described in methodology section. From the results (Table 5, Fig. 8a–d), it is clear that for Cr(VI) removal kinetics data followed by pseudo-second-order kinetics model for both the adsorbents with the value of coefficient of correlation ( $R^2$ ) 0.9956 for  $\text{BC}_{\text{PH}}$  and 0.9998 for  $\text{MBC}_{\text{PH}}$ . The  $q_e$  value obtained from pseudo-second-order kinetic model was 5.83 mg/g and 11.97 mg/g for  $\text{BC}_{\text{PH}}$  and  $\text{MBC}_{\text{PH}}$ , respectively, which are approximately nearer to the experimental  $q_e$  value.

### 3.5 Thermodynamic Study

Thermodynamic study was conducted to look on the effect of temperature on Cr(VI) adsorption onto the adsorbents ( $\text{MBC}_{\text{PH}}$  and  $\text{BC}_{\text{PH}}$ ). Based on the Van't Hoff equation Gibbs free energy ( $\Delta G^0$ , kJ/mol), enthalpy ( $\Delta H^0$ , kJ/mol) and entropy ( $\Delta S^0$ , J/mol. K) were calculated. Thermodynamic parameter can be calculated based on the following Eq. (16) and (17) [32]:

$$\Delta G^0 = -RT \ln K_c \quad (16)$$

**Fig. 6** **a** Langmuir, **b** Freundlich and **c** Temkin adsorption isotherm model for the sorption of Cr(VI) onto MBC<sub>PH</sub> and BC<sub>PH</sub>

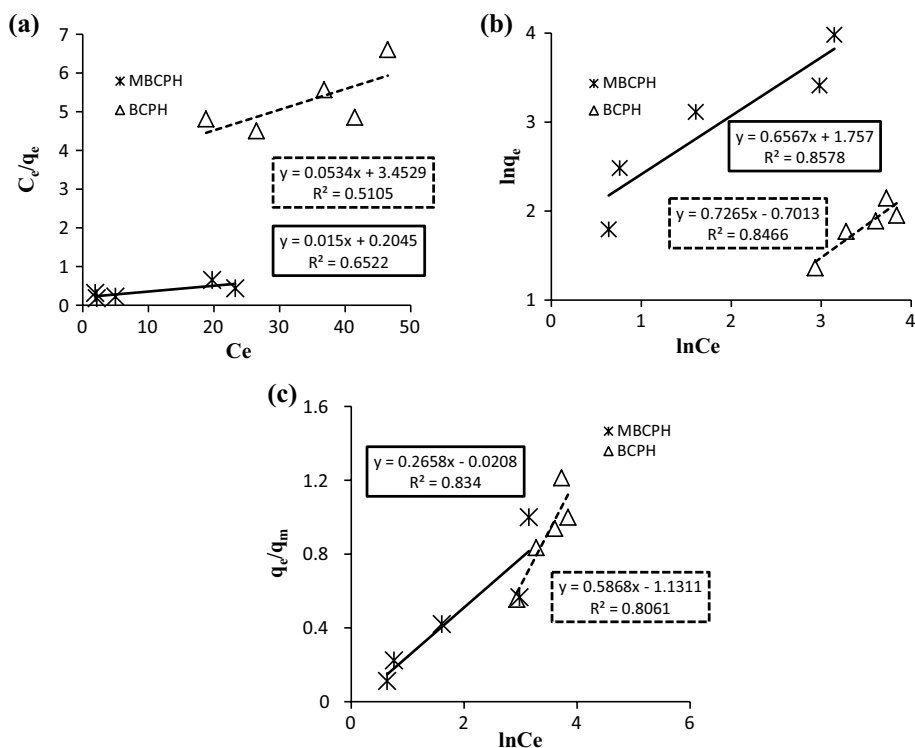


**Fig. 7** Dubinin–Radushkevich (D–R) model for sorption of Cr(VI) onto **a** MBC<sub>PH</sub> and **b** BC<sub>PH</sub>

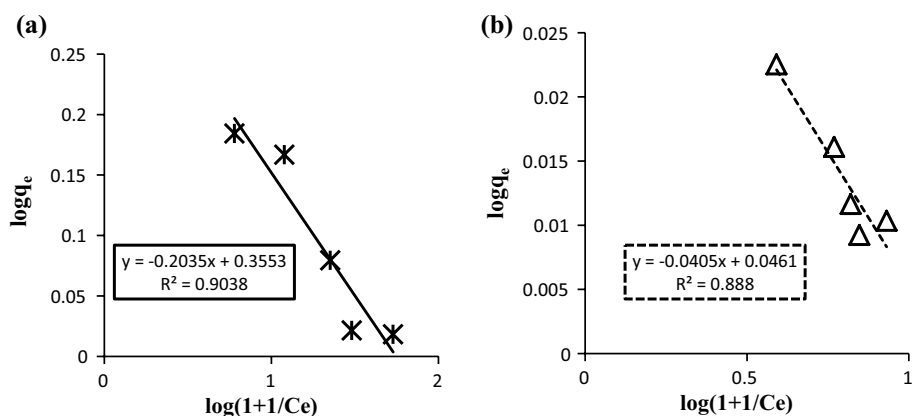


**Table 4** Dubinin–Radushkevich (D–R) model constants and correlation coefficient data

Adsorbents	$q_D$ (mg g <sup>-1</sup> )	$B_D$ (mol <sup>2</sup> kJ <sup>-2</sup> )	$E_D$ (kJ mol <sup>-1</sup> )	$R^2$
BC <sub>PH</sub>	1.0472	0.0033	0.0813	0.888
MBC <sub>PH</sub>	2.2663	0.0166	5.492	0.9038

$$\Delta G^0 = \Delta H^0 - T\Delta S^0 \tag{17}$$

where  $T$  represents as sorption temperature and  $R$  represents as universal gas constant (8.314 J mol<sup>-1</sup> K<sup>-1</sup>). By the following Eq. (18)  $K_c$  may be expressed as a function of temperature [32].

$$\ln K_c = -\frac{\Delta H^0}{RT} + \frac{\Delta S^0}{R} \tag{18}$$

From the Van't Hoff plot (Fig. 9a,b) of  $K_c$  versus  $1/T$ , the values of  $\Delta H^0$  and  $\Delta S^0$  can be evaluated.

Thermodynamic study gives an idea about the adsorption nature. Thermodynamic results are summarized in Table 6. It can be seen that the value of Gibbs free energy ( $\Delta G^0$ ) within the temperature ranges (15° to 45 °C) are negative for both adsorbents (MBC<sub>PH</sub> and BC<sub>PH</sub>). This indicated that the sorption of Cr(VI) was spontaneous and energy was generated within the system. The  $\Delta G^0$  value decreased with increased in temperature which revealed that high temperature favoured the sorption process of Cr(VI) for both the adsorbents as shown in Fig. 5. For both the adsorbents, the

**Table 5** Comparison between adsorption rate constants and correlation coefficients of kinetic models

Kinetic models	Parameters	Adsorbents	
		BC <sub>PH</sub>	MBC <sub>PH</sub>
Pseudo-first-order reaction model	$K_1$ (min <sup>-1</sup> )	0.017	0.029
	$R^2$	0.9765	0.9149
Pseudo-second-order reaction model	$K_2$ (g mg <sup>-1</sup> min <sup>-1</sup> )	0.0166	0.0656
	$R^2$	0.9956	0.9998
Weber and Morris equation	$k_d$ (mgg <sup>-1</sup> min <sup>-1/2</sup> )	3.1743	5.0716
	$R^2$	0.9464	0.739
Elovich equation	$\alpha$ (mg g <sup>-1</sup> min <sup>-1</sup> )	1.374	9.7642
	$\beta$ (gmg <sup>-1</sup> )	0.7927	0.4337
	$R^2$	0.954	0.9333

**Fig. 8** **a** Pseudo-first-order, **b** Pseudo-second-order, **c** Weber and Morris and **d** Elovich kinetic model for the sorption of Cr(VI) onto MBC<sub>PH</sub> and BC<sub>PH</sub>

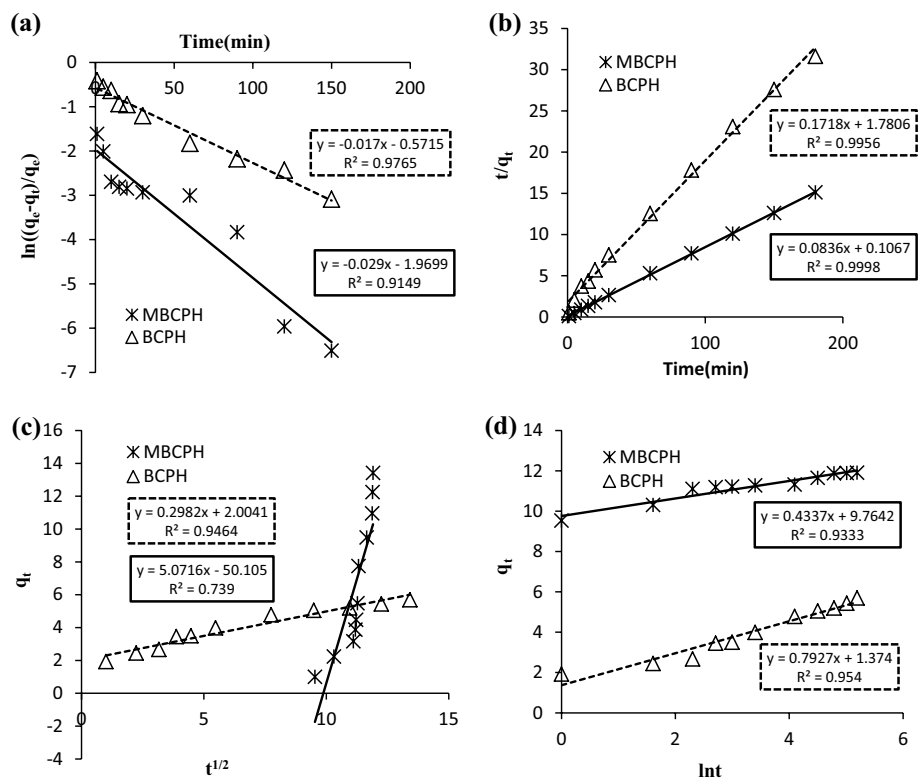


**Fig. 9** Van't Hoff plot for the sorption of Cr(VI) onto **a** MBC<sub>PH</sub> and **b** BC<sub>PH</sub>

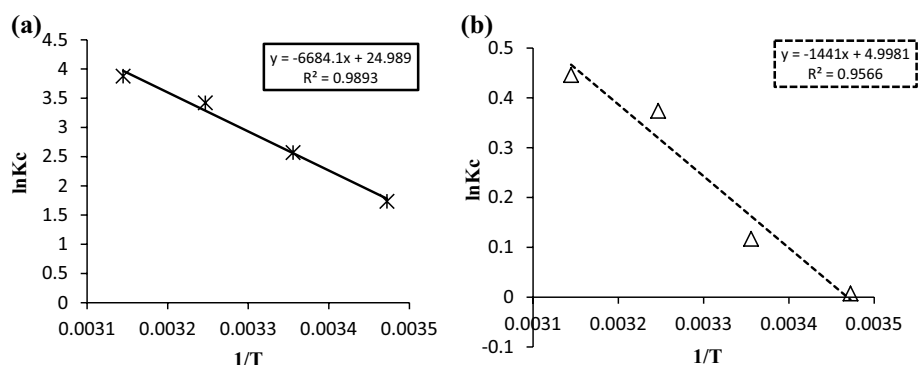


**Table 6** Thermodynamics parameters evaluation for sorption of Cr(VI) onto MBC<sub>PH</sub> and BC<sub>PH</sub>

Temperature(K)	BC <sub>PH</sub>			MBC <sub>PH</sub>		
	$\Delta G^0$ (kJ mol <sup>-1</sup> )	$\Delta H^0$ (kJ mol <sup>-1</sup> )	$\Delta S^0$ (J mol <sup>-1</sup> K <sup>-1</sup> )	$\Delta G^0$ (kJ mol <sup>-1</sup> )	$\Delta H^0$ (kJ mol <sup>-1</sup> )	$\Delta S^0$ (J mol <sup>-1</sup> K <sup>-1</sup> )
288	-0.02	11.98	41.56	-4.26	55.58	207.76
298	-0.29			-6.34		
308	-0.96			-8.42		
318	-1.18			-10.49		

$\Delta S^0$  value was positive which indicates the increasing randomness during the adsorption process between Cr(VI) and the adsorbents. As well as, the positive value of  $\Delta H^0$  for both the adsorbents revealed that the Cr(VI) adsorption process is endothermic in nature [33].

### 3.6 Effect of Coexisting Ions on Cr (VI) Adsorption

In general, wastewater contains several ions (anions and cations) and those effects on the removal of Cr (VI). So it is necessary to study the influence of co-ions on the adsorption process of Cr(VI) on to the biochar surface. This study was conducted only with MBC<sub>PH</sub> because this adsorbent shows better affinity for Cr(VI) compared to BC<sub>PH</sub>. In this study three common major cations (Na<sup>+</sup>, Mg<sup>2+</sup>, and Al<sup>3+</sup>) and four common anions (Cl<sup>-</sup>, HCO<sub>3</sub><sup>-</sup>, SO<sub>4</sub><sup>2-</sup> and PO<sub>4</sub><sup>3-</sup>) were examined to observe the coexisting ionic effects on the adsorption of Cr(VI). Figure 10 delineated that, the adsorption process of Cr(VI) was not significantly affected in the presence of cations (Na<sup>+</sup>, Mg<sup>2+</sup>, Al<sup>3+</sup>). This may be due to the electrostatic repulsion. Under the experimental conditions (pH<sub>solution</sub> < pH<sub>zpc</sub>), repulsion between the positively surface charged biochar and positively charged cations could prevent the cations from being adsorb onto the surface of the adsorbent. Therefore, there was no competition between Cr(VI) ions and the major cations in the sorption process [34]. From the result, it has been observed that there was slight interference of cations on Cr(VI) removal and the interference is directly proportional to the size of the cations or solubility of the electrolytes and follows the order Al<sup>3+</sup> < Mg<sup>2+</sup> < Na<sup>+</sup>.

In order to determine the anionic effect on adsorption process of Cr(VI) common anions (Cl<sup>-</sup>, HCO<sub>3</sub><sup>-</sup>, SO<sub>4</sub><sup>2-</sup> and PO<sub>4</sub><sup>3-</sup>) were taken. The anions Cl<sup>-</sup>, HCO<sub>3</sub><sup>-</sup>, SO<sub>4</sub><sup>2-</sup> and PO<sub>4</sub><sup>3-</sup> provide the anionic charges are -1, -1, -2, -3. From Fig. 11 it can be seen that the adsorption process of Cr(VI) was highly affected due to the presence of anions. Competition of anions with hexavalent chromium for the adsorption should mainly arise due to the similar ionic nature. This may be due to the electrostatic attraction. Under the experimental conditions (pH<sub>solution</sub> < pH<sub>zpc</sub>) attraction between the positively surface charged biochar and negatively charged anions affect the removal of Cr(VI). It has been observed that under experimental concentration ranges Cl<sup>-</sup> ion has

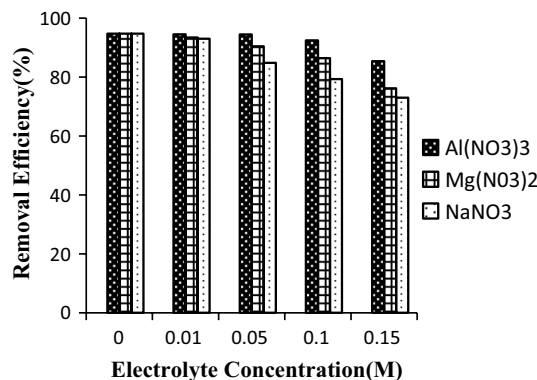


**Fig. 10** Effect of co-cations on removal of Cr(VI) by MBC<sub>PH</sub>

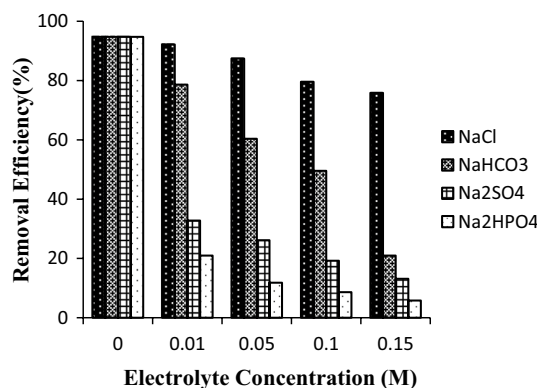


**Fig. 11** Effect of co-anions on removal of Cr(VI) by MBC<sub>PH</sub>

less impact on Cr(VI) removal. In the case of HCO<sub>3</sub><sup>-</sup> ion, it was observed that Cr(VI) removal was affected in the higher concentration of bicarbonate(HCO<sub>3</sub><sup>-</sup>) ions. This can be explained as, due to the hydrolysis bicarbonate ions releases OH<sup>-</sup> ions which might increases the solution pH and decrease the removal efficiency of Cr(VI) ions [35]. The presence of sulfate (SO<sub>4</sub><sup>2-</sup>) ions hindered the removal of Cr(VI) ions on to the adsorbent surfaces. In the presence of SO<sub>4</sub><sup>2-</sup> ions adsorption capacity reduced may be due to the formation of complexes on the surface of the adsorbent. The presence of phosphate (PO<sub>4</sub><sup>3-</sup>) ions showed the greatest impact in Cr(VI) sorption on to the adsorption surfaces. This may be explained as the size and structure of PO<sub>4</sub><sup>3-</sup> ions is

similar to  $\text{HCrO}_4^-$  and  $\text{CrO}_4^{2-}$  ions. Therefore, competition of  $\text{PO}_4^{3-}$  ions with hexavalent chromium for active sites on the surface of the adsorbent reduced the removal capacity of Cr(VI). From the result it has been observed that the interference is directly proportional to the charge on the anions and follow the order  $\text{Cl}^- < \text{HCO}_3^- < \text{SO}_4^{2-} < \text{PO}_4^{3-}$ .

### 3.7 Regeneration Study

The regeneration study was carried out to check the recyclability potential of the adsorbent, which improve the economics of waste water treatment. Recyclability is an important factor by which as a researcher we can understand how many times the adsorbent can be reused. On the other hand, it is not safe to dispose the saturated adsorbent which contains Cr(VI) [21]. To minimize the environmental impact from the spent adsorbent, the Cr(VI) loaded adsorbent was regenerated. In this study, after adsorption  $\text{MBC}_{\text{PH}}$  was easily separated by using an external magnetic field as shown in Fig. 1.  $\text{MBC}_{\text{PH}}$  showed good recyclability when 0.1 M NaOH used as a desorbing solution. After regeneration by NAOH solution 0.2 g of  $\text{MBC}_{\text{PH}}$  was applied at 50 ml of 50 mg/L of Cr(VI) solution. This recycling process was continued up to 4th cycle. From Fig. 12, it can be seen that after the first regeneration cycle the Cr(VI) removal efficiency decrease from 96.22 to 89.90%. After the third regeneration cycle, the removal efficiency of Cr(VI) was maintained at 71.79%. But after the third regeneration cycle the removal efficiency of Cr(VI) was decreased to 56.03%. The results revealed that up to the fourth regeneration cycles  $\text{MBC}_{\text{PH}}$  could maintain high adsorption performance. Consequently, it can be concluded that  $\text{MBC}_{\text{PH}}$  could be recycled and maintain higher adsorption capacity. The decrease in adsorption performance of  $\text{MBC}_{\text{PH}}$  may be due to: (1) during the regeneration process some pores on the adsorbent surface might be blocked; (2) reduction in the number of available active adsorption sites on the adsorbent due to the formation of complex between Cr(VI) and functional groups. This study

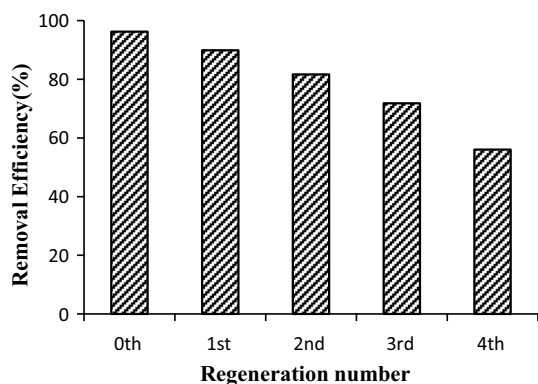


Fig. 12 Regeneration of  $\text{MBC}_{\text{PH}}$  for Cr(VI) removal

was conducted only for  $\text{MBC}_{\text{PH}}$  as it shows higher adsorption capacity for Cr(VI) removal (Fig. 13).

## 4 Mechanism

Freundlich isotherm model demonstrate heterogeneous sorption process for Cr(VI) removal for both the adsorbents. The adsorption mechanism was mainly dependent on solution pH and point of zero charge (pH<sub>zpc</sub>) of the synthesized materials. As briefly discussed in Sect. 3.2.4, at very low solution pH Cr(VI) is electrostatically adsorbed on to the surface of the biochar. Hence, electrostatic attraction is one possible reason behind the adsorption process of Cr(VI). In contrast, as discussed in Sect. 3.1, the literature revealed that various oxygen containing functional groups are presents on the surface of  $\text{MBC}_{\text{PH}}$  and  $\text{BC}_{\text{PH}}$ . Reduction of Cr(VI) to Cr(III) (See Eq. 14 and 15) by oxygen-containing functional groups, subsequently Cr(III) complexation with oxygen-containing functional groups on the adsorbent is another possible mechanism. Also abundant pores and high specific surface area involved in the higher removal process of Cr(VI).

## 5 Conclusion

In the present study, magnetic biochar has been developed using peanut husk for the removal of Cr(VI) from aqueous solution. During the characterization of the adsorbent, it is revealed that the BET Surface area of biochar was increased from 16.48 to 183.62  $\text{m}^2/\text{g}$  after magnetization with iron oxides due to dope of the iron oxides nanoparticles on to the surface of biochar. The sorption of Cr(VI) significantly affected by the solution pH and the surface structure of the adsorbent. Furthermore, due to the variance of free energy and the available active adsorption sites, temperature and dosage also impacted on the sorption of Cr(VI). The Thermodynamic study shows that the sorption process is

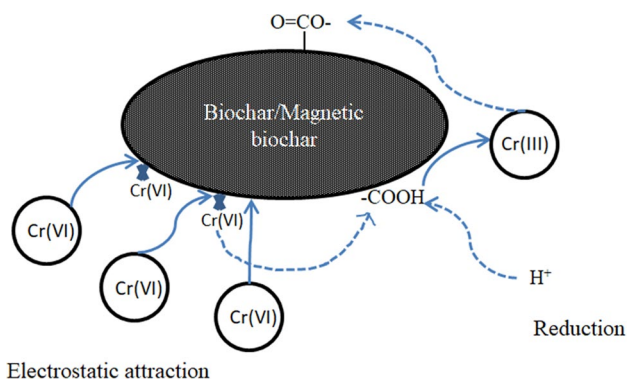


Fig. 13 Possible removal mechanism of Cr(VI) by  $\text{BC}_{\text{PH}}$  and  $\text{MBC}_{\text{PH}}$

spontaneous and endothermic in nature. From the obtained result, it can be seen that the removal efficiency of Cr (VI) was decreased with the increase of pH of the solution. It may be possible that as Cr(VI) present in aqueous solution in different ionic forms, such as  $\text{HCrO}_4^-$ ,  $\text{Cr}_2\text{O}_7^{2-}$ , and  $\text{CrO}_4^{2-}$ , which directly depends on the redox condition of the solution and the concentration level of Cr (VI) ions. From the kinetic study, it can be seen that the removal efficiency of Cr(VI) ions reaches up to 95.27% for  $\text{MBC}_{\text{PH}}$  and 45.56% for  $\text{BC}_{\text{PH}}$  respectively within 180 min. The adsorption process for  $\text{MBC}_{\text{PH}}$  was controlled by film diffusion process and within 20 min the removal efficiency reached to 90%. The adsorption capacity obtained from the result was 8.507 mg/g and 75.656 mg/g for  $\text{BC}_{\text{PH}}$  and  $\text{MBC}_{\text{PH}}$ , respectively. From the study of effect of coexisting ions, it can be seen that there was slight interference of cations on Cr(VI) removal and the interference is directly proportional to the size of the cations or solubility of the electrolytes and follows the order  $\text{Al}^{3+} < \text{Mg}^{2+} < \text{Na}^+$ . Formation of  $\gamma\text{-Fe}_2\text{O}_3$  on the surface of  $\text{MBC}_{\text{PH}}$  contributed to much higher removal efficiency compared to the standard biochar ( $\text{BC}_{\text{PH}}$ ). Moreover, higher removal efficiency was maintained up to the third regeneration cycle. In contrast, presence of  $\text{HCO}_3^-$ ,  $\text{SO}_4^{2-}$  and  $\text{PO}_4^{3-}$  anions affected the removal capacity of  $\text{MBC}_{\text{PH}}$ . However, higher removal efficiency was maintained up to the third regeneration cycle. This study provided a promising adsorbent for the separation of Cr(VI) from aqueous solution.

**Author contributions** Byomkesh Mahanty performed the batch study, kinetic study, isotherm study, thermodynamic study, interpreted the rate of reaction and types of adsorption and was a major contributor in writing the manuscript. Sandip Mondal analyzed the data and wrote the manuscript.

**Funding** This work was supported by grants from the Department of Science & Technology and Biotechnology, Government of West Bengal (Memo No. 231(Sanc.)/ST/P/S&T/5G-19/2017 dated 24/03/2018).

**Data Availability** The datasets used and analyzed during the current study are available from the corresponding author on reasonable request.

## Declarations

**Conflict of interests** The authors declare that they have no competing interests.

## References

- Zhu, S.; Huang, X.; Wang, D.; Wang, L.; Ma, F.: Enhanced hexavalent chromium removal performance and stabilization by magnetic iron nanoparticles assisted biochar in aqueous solution: mechanisms and application potential. *Chemosphere* **207**, 50–59 (2018)
- Cai, W.; Gu, M.; Jin, W.; Zhou, J.: CTAB-functionalized C@SiO<sub>2</sub> double-shelled hollow microspheres with enhanced and selective adsorption performance for Cr (VI). *J. Alloy. Compd.* **777**, 1304–1312 (2019)
- Cai, W.; Wei, J.; Li, Z.; Liu, Y.; Zhou, J.; Han, B.: Preparation of amino-functionalized magnetic biochar with excellent adsorption performance for Cr (VI) by a mild one-step hydrothermal method from peanut hull. *Colloids. Surf. A.* **563**, 102–111 (2019)
- Li, H.; Dong, X.; da Silva, E.B.; de Oliveira, L.M.; Chen, Y.; Ma, L.Q.: Mechanisms of metal sorption by biochars: biochar characteristics and modifications. *Chemosphere* **178**, 466–478 (2017)
- Son, E.B.; Poo, K.M.; Chang, J.S.; Chae, K.J.: Heavy metal removal from aqueous solutions using engineered magnetic biochars derived from waste marine macro-algal biomass. *Sci. Total. Environ.* **615**, 161–168 (2018)
- Dong, X.; Ma, L.Q.; Li, Y.: Characteristics and mechanisms of hexavalent chromium removal by biochar from sugar beet tailing. *J. Hazard. Mater.* **190**(1–3), 909–915 (2011)
- Agrafioti, E.; Kalderis, D.; Diamadopoulos, E.: Arsenic and chromium removal from water using biochars derived from rice husk, organic solid wastes and sewage sludge. *J. Environ. Manag.* **133**, 309–314 (2014)
- Han, Y.; Cao, X.; Ouyang, X.; Sohi, S.P.; Chen, J.: Adsorption kinetics of magnetic biochar derived from peanut hull on removal of Cr (VI) from aqueous solution: effects of production conditions and particle size. *Chemosphere* **145**, 336–341 (2016)
- Ma, Y.; Liu, W.J.; Zhang, N.; Li, Y.S.; Jiang, H.; Sheng, G.P.: Polyethylenimine modified biochar adsorbent for hexavalent chromium removal from the aqueous solution. *Biores. Technol.* **169**, 403–408 (2014)
- Pan, J.J.; Jiang, J.; Xu, R.K.: Removal of Cr (VI) from aqueous solutions by Na<sub>2</sub>SO<sub>3</sub>/FeSO<sub>4</sub> combined with peanut straw biochar. *Chemosphere* **101**, 71–76 (2014)
- Evbuomwan, B.O.; Alalibo, J.T.: Proximate and ultimate analysis of walnut shell as a potential low cost adsorbent using different activating agents (KOH and H<sub>2</sub>SO<sub>4</sub>). *Chem. Res. J.* **2**(5), 124–130 (2018)
- Lowell, S.; Shields, J.E.: Powder Surface Area and Porosity, Vol. 2. Springer, New York (2013)
- Kumar, R.; Mondal, S.: Removal of fluoride from aqueous solution using coal-coated with FeCl<sub>3</sub>. In: *Recent Developments in Waste Management*, pp. 417–434. Springer, Singapore (2020)
- Verma, L.; Siddique, M.A.; Singh, J.; Bharagava, R.N.: As (III) and As (V) removal by using iron impregnated biosorbents derived from waste biomass of Citrus limmeta (peel and pulp) from the aqueous solution and ground water. *J. Environ. Manag.* **250**, 109452 (2019)
- Langmuir, I.: The adsorption of gases on plane surfaces of glass, mica and platinum. *J. Am. Chem. Soc.* **40**(9), 1361–1403 (1918)
- Freundlich, H.: Über die adsorption in lösungen. *Z. Phys. Chem.* **57**(1), 385–470 (1907)
- Temkin, M.J., Pyzhev, V. Recent modifications to Langmuir isotherms. (1940)
- Dubin, M. M. (1947). The equation of the characteristic curve of activated charcoal. In: *Dokl. Akad. Nauk. SSSR*, vol. 55, pp. 327–329
- Garg, U.K.; Kaur, M.P.; Garg, V.K.; Sud, D.: Removal of hexavalent chromium from aqueous solution by agricultural waste biomass. *J. Hazard. Mater.* **140**(1–2), 60–68 (2007)
- Yang, X.; Al-Duri, B.: Kinetic modeling of liquid-phase adsorption of reactive dyes on activated carbon. *J. Colloid. Interface. Sci.* **287**(1), 25–34 (2005)
- Gupta, S.; Babu, B.V.: Removal of toxic metal Cr (VI) from aqueous solutions using sawdust as adsorbent: equilibrium, kinetics and regeneration studies. *Chem. Eng. J.* **150**(2–3), 352–365 (2009)



22. Davarnejad, R.; Dastnayi, Z.K.; Kennedy, J.F.: Cr (VI) adsorption on the blends of Henna with chitosan microparticles: Experimental and statistical analysis. *Int. J. Biol. Macromol.* **116**, 281–288 (2018)
23. Bansal, M.; Garg, U.; Singh, D.; Garg, V.K.: Removal of Cr (VI) from aqueous solutions using pre-consumer processing agricultural waste: a case study of rice husk. *J. Hazard. Mater.* **162**(1), 312–320 (2009)
24. Kooh, M.R.R.; Dahri, M.K.; Lim, L.B.: Removal of the methyl violet 2B dye from aqueous solution using sustainable adsorbent *Artocarpus odoratissimus* stem axis. *Appl. Water. Sci.* **7**(7), 3573–3581 (2017)
25. Mondal, S.; Mahanta, C.: Evaluation of arsenic adsorption capacity of indigenous materials for their suitability as filter media. *Desalin. Water. Treat* **84**, 309–323 (2017)
26. Chien, S.H.; Clayton, W.R.: Application of Elovich equation to the kinetics of phosphate release and sorption in soils I. *Soil. Sci. Soc. Am. J.* **44**(2), 265–268 (1980)
27. Ho, Y.S.; McKay, G.: A comparison of chemisorption kinetic models applied to pollutant removal on various sorbents. *Trans. IChemE.* **76**(4), 332–340 (1998)
28. Ho, Y.S.; McKay, G.: Comparative sorption kinetic studies of dye and aromatic compounds onto fly ash. *J. Environ. Sci. Health. Part. A.* **34**(5), 1179–1204 (1999)
29. Soliemanzadeh, A.; Fekri, M.: The application of green tea extract to prepare bentonite-supported nanoscale zero-valent iron and its performance on removal of Cr (VI): effect of relative parameters and soil experiments. *Microporous. Mesoporous. Mater.* **239**, 60–69 (2017)
30. Zhao, H.; Lang, Y.: Adsorption behaviors and mechanisms of florfenicol by magnetic functionalized biochar and reed biochar. *J. Taiwan. Inst. Chem. Eng.* **88**, 152–160 (2018)
31. Fan, Y.; Yang, R.; Lei, Z.; Liu, N.; Lv, J.; Zhai, S.; Wang, L.: Removal of Cr (VI) from aqueous solution by rice husk derived magnetic sorbents. *Korean. J. Chem. Eng.* **33**(4), 1416–1424 (2016)
32. Vithanage, M.; Mayakaduwa, S.S.; Herath, I.; Ok, Y.S.; Mohan, D.: Kinetics, thermodynamics and mechanistic studies of carbofuran removal using biochars from tea waste and rice husks. *Chemosphere* **150**, 781–789 (2016)
33. Njoku, V.O.; Islam, M.A.; Asif, M.; Hameed, B.H.: Preparation of mesoporous activated carbon from coconut frond for the adsorption of carbofuran insecticide. *J. Anal. Appl. Pyrol.* **110**, 172–180 (2014)
34. Ma, H.; Yang, J.; Gao, X.; Liu, Z.; Liu, X.; Xu, Z.: Removal of chromium (VI) from water by porous carbon derived from corn straw: Influencing factors, regeneration and mechanism. *J. Hazard. Mater.* **369**, 550–560 (2019)
35. Periyasamy, S.; Gopalakannan, V.; Viswanathan, N.: Fabrication of magnetic particles imprinted cellulose based biocomposites for chromium (VI) removal. *Carbohydr. Polym.* **174**, 352–359 (2017)
36. Ahmad, M.; Lee, S.S.; Dou, X.; Mohan, D.; Sung, J.K.; Yang, J.E.; Ok, Y.S.: Effects of pyrolysis temperature on soybean stover and peanut shell-derived biochar properties and TCE adsorption in water. *Biores. Technol.* **118**, 536–544 (2012)
37. Aryee, A.A.; Mpatani, F.M.; Zhang, X.; Kani, A.N.; Dovi, E.; Han, R.; Li, Z.; Qu, L.: Iron (III) and iminodiacetic acid functionalized magnetic peanut husk for the removal of phosphate from solution: characterization, kinetic and equilibrium studies. *J. Clean. Prod.* (2020). <https://doi.org/10.1016/j.jclepro.2020.122191>
38. Lingamdinne, L.P.; Lee, S.; Choi, J.S.; Lebaka, V.R.; Durbaka, V.R.P.; Koduru, J.R.: Potential of the magnetic hollow sphere nanocomposite (graphene oxide-gadolinium oxide) for arsenic removal from real field water and antimicrobial applications. *J. Hazard. Mater.* (2021). <https://doi.org/10.1016/j.jhazmat.2020.123882>
39. Lingamdinne, L.P.; Choi, J.S.; Choi, Y.L.; Yang, J.K.; Koduru, J.R.; Chang, Y.Y.: Green activated magnetic graphitic carbon oxide and its application for hazardous water pollutants removal. *Metals* (2019). <https://doi.org/10.3390/met9090935>
40. Liu, Y.; Sohi, S.P.; Liu, S.; Guan, J.; Zhou, J.; Chen, J.: Adsorption and reductive degradation of Cr (VI) and TCE by a simply synthesized zero valent iron magnetic biochar. *J. Environ. Manag.* **235**, 276–281 (2019)
41. Mishra, S.; Yadav, S.S.; Rawat, S.; Singh, J.; Koduru, J.R.: Corn husk derived magnetized activated carbon for the removal of phenol and para-nitrophenol from aqueous solution: Interaction mechanism, insights on adsorbent characteristics, and isothermal, kinetic and thermodynamic properties. *J Environ. Manag.* (2019). <https://doi.org/10.1016/j.jenvman.2019.06.013>

